Sequential Deconstruction-Reconstruction of Metal-Organic Frameworks: an Alternative Strategy for Synthesizing (Multi)-Layered ZIF Composites

Civan Avci,[†] Amirali Yazdi,[†] Màrius Tarrés,[‡] Elise Bernoud,[‡] Neus G. Bastús,[†] Victor Puntes,[†,§] Inhar Imaz,[†] Xavi Ribas[‡] and Daniel Maspoch[*,†,§]

[†] Catalan Institute of Nanoscience and Nanotechnology (ICN2), CSIC and The Barcelona Institute of Science and Technology, Campus UAB, Bellaterra, 08193 Barcelona, Spain

[‡] Institut de Química Computacional i Catàlisi (IQCC) and Departament de Química, Universitat de Girona, Campus Montilivi, Girona, E-17071, Catalonia, Spain

[§] ICREA, Pg. Lluís Companys 23, 08010 Barcelona, Spain

ABSTRACT: Here we report the synthesis of (multi)-layered Zeolitic Imidazolate Framework (ZIF-8/-67) composite particles *via* a sequential deconstruction-reconstruction process. We show that this process can be applied to construct ZIF-8-on-ZIF-67 composite particles whose cores are the initially etched particles. In addition, we demonstrate that introduction of functional inorganic nanoparticles (INPs) onto the crystal surface of etched particles does not disrupt ZIF particle reconstruction, opening new avenues for designing (multi)-layered ZIF-on-INP-on-ZIF composite particles comprising more than one class of inorganic nanoparticles. In these latter composites, the location of the inorganic nanoparticles inside each single MOF particle as well as of their separation at the nanoscale (20 nm) is controlled. Preliminary results show that (multi)-layered ZIF-on-INP-on-ZIF composite particles comprising a good sequence of inorganic nanoparticles can potentially catalyze cascade reactions.

KEYWORDS: metal-organic frameworks, inorganic nanoparticles, ZIF composites, etching, crystal growth, cascade catalysis

INTRODUCTION

A major obstacle to the practical application of diverse nanomaterials is the lack of methods to control their morphology.[1, 2] To date, several top-down (*e.g.* etching, lithography, etc.)[3-5] and bottom-up (*e.g.* use of surfactants, controlled self-assembly, etc.)[6-8] approaches have been employed to design nanomaterials with specific shapes. However, most advanced nanomaterials are not produced and shaped in a single step but rather consecutively, via top-down and bottom-up strategies. A well-known example is the production of integrated circuits[9], whereby multiple steps of material deposition (bottom-up) are followed by consecutive photolithographic processes (top-down) in order to reach complex patterns of heterogeneous composition. In the field of inorganic nanoparticles (INPs), a common approach is to combine oxidative etching (top-down) with growth methods (bottom-up), which yields nanoparticles with unprecedented shapes.[10-13]

Recent efforts to control the growth of metal-organic framework (MOF) particles have aimed at discovering new shapes[14] and at making more complex, multicomponent (composite) particles, built by growing one MOF on top of another (known as MOF-on-MOF systems)[15, 16] and by combining MOFs with other functional materials such as INPs[17-19] and biosystems.[20-22] Among the many reported MOFs, the most studied case by far is that of the zeolitic imidazolate frameworks ZIF-8 and ZIF-67, which are isostructural porous materials (S_{BET} ~ 1400-1700 m^2/g) made of Zn(II) and Co(II) ions, respectively. Each ZIF is very interesting because one can epitaxially grow on top of the other one (bottom-up) to afford either ZIF-8-on-ZIF-67 or ZIF-67-on-ZIF-8 particles.[23-26] Also, ZIF-8/ZIF-67 particles can be etched (top-down) into novel shapes[27, 28] or synthesized as hollow or yolk-shelled particles.[29-34] Furthermore, both of these ZIFs can grow on the surface of INPs and biosystems, meaning that a rich variety of core-shell[35-44] and layered composites[17, 23, 45] could be designed.

With these advances, both MOF-on-MOF and etching approaches are now being combined, either sequentially (in said order) or simultaneously, to afford new ZIF-8/ZIF-67 particles. For instance, Li *et al.* and Muhler, Fischer *et al.* reported formation of hollow Zn/Co ZIF particles in which ZIF-8-on-ZIF-67 particles were built and then, the ZIF-67 core was etched due to its lower stability in MeOH compared to ZIF-8 under mild solvothermal conditions.[46,47] Similarly, Tsung *et al.* have shown that pre-formed ZIF-8 particles could be simultaneously regrown and etched to create hollow ZIF-8 particles.[31] And very recently, Liu, Huo *et al.* have applied regrowth processes followed by etching to build multi-shelled hollow particles of the well-known MIL-101.[29]

Herein, we report a novel strategy to construct ZIF-on-ZIF and (multi)-layered ZIF-on-INP-on-ZIF particles. Unlike the aforementioned combination (bottom-up/top-down) methods, our method begins with controlled etching followed by MOF-

on-MOF growth. Recently, we have demonstrated that colloidal ZIF-8 and ZIF-67 particles can be anisotropically etched into well-defined, unprecedented morphologies. With this deconstructive method, truncated rhombic dodecahedral (tRD) and rhombic dodecahedral (RD) particles can be transformed into uniform cubic (C), hollow (H) or tetrahedral (T) particles (Figure S1). We show that these etched ZIF-8/-67 particles can be reversibly reconstructed to their initial shapes. This reconstruction entails growing ZIF-8 on the etched particles. Therefore, the sequential deconstruction-reconstruction process can be used to form ZIF-8-on-ZIF-67 particles whose cores are the initially etched particles. In addition, we demonstrate that the inclusion of functional INPs on the crystal surface of etched particles does not disrupt particle reconstruction. This observation opens the possibility of using this sequential process to design (multi)-layered ZIF-on-INP-on-ZIF composites formed by more than one class of INPs. In these onion-like composites, the sequence of the INPs can be controlled from outside to inside the ZIF crystal, paving the way for using them for innovative cascade catalytic reactions.

EXPERIMENTAL SECTION

Materials. All materials were purchased from Sigma-Aldrich with no further modification.

Synthesis of tRD_{ZIF-67}, RD_{ZIF-67} and tRD_{ZIF-8} particles. A solution of 0.6 g of $Co(OAc)_2 \cdot 4H_2O$ in 5 mL of DI water was added into a solution of 2.24 g of 2-methylimidazole (2-MiM) in 5 mL of deionized (DI) water, and the resulting mixture was homogenized by stirring for a few seconds. Then, the mixture was let at room temperature for 10 min to form tRD_{ZIF-67} particles. RD_{ZIF-67} particles were prepared using the same procedure as for the truncated ones, except that the mixture was let for 5 h at room temperature. In both cases, purple crystals were collected and washed several times with methanol. Finally, the powder was dried under vacuum for 5 h at room temperature. In the case of tRD_{ZIF-8} particles, a solution of 0.3 g of $Zn(OAc)_2 \cdot 2H_2O$ in 5 mL of DI water was added into a solution of 1.12 g of 2-MiM in 5 mL of DI water, and the resulting mixture was homogenized by stirring for a few seconds. Then, the mixture was let at room temperature for 5 h to form tRD_{ZIF-8} particles.

General route for etching ZIF-67 particles. The general method starts with the preparation of a colloidal ZIF-67 solution by ultrasonication of 25 mg of tRD or RD ZIF-67 particles in 2.5 mL of DI water for 15 min. In parallel, 40 mg of xylenol orange (XO) was dissolved in 2.5 mL of DI water, and the *pH* of this etchant solution was adjusted by adding HCl or NaOH. Note here that the etching solution in this process is acidified/basified XO, which protonates the 2-MiM linkers, breaks the coordination bonds and sequesters the liberated Co(II) ions. The colloidal solution was then injected into the etchant solution, and the resulting mixture was stirred at 300 rpm for an optimized time (*t*). The final solid was collected by centrifugation and washed several times using methanol. The specific conditions for each etching process were: C_{ZIF-67}: pH = 8.0 and t = 3 h; and T_{ZIF-67}: pH = 3.5 and t = 3 h. Note here that, only for T_{ZIF-67}, a second etching step was needed to obtain a uniform sample. This second etching step consisted on washing the primarily etched crystals with water, re-dispersing them in 1 mL of DI water, and incubating them with 1 mL of XO etchant solution at pH = 5.80 for 30 min.

General route for growing ZIF-8-on-ZIF-67 particles. The general method started with the preparation of a colloidal ZIF-67 solution by ultrasonication of 5 mg of core ZIF-67 particles in 5 mL of methanol for 15 min. 2.5 mL of 2-MiM and 2.5 mL of $Zn(NO_3)_2 \cdot 6H_2O$ with varying concentrations (C) were added to the colloidal solution, and the resulting mixture was let at room temperature for a time t. Finally the re-grown particles were collected by centrifugation and washing steps with methanol. To make RD_{ZIF-8}-on-ZIF-67 crystals with C_{ZIF-67} or T_{ZIF-67} core: C = 25 mM, t = 1 day; and with H_{ZIF-67} core: C = 25 mM, t = 4 days. To make tRD_{ZIF-8}-on-ZIF-67 crystals with C_{ZIF-67} or T_{ZIF-67} core: C = 10 mM, t = 1 day; and with H_{ZIF-67} intermediate: C = 25 mM, t = 1 day.

Synthesis of Au nanoparticles (~9 nm diameter). Au NPs were produced following a previously reported protocol.[48] In detail, a solution of 2.2 mM sodium citrate in DI water (150 mL) was heated with a heating mantle in a 250 mL three-necked round-bottomed flask for 15 min under vigorous stirring. A condenser was utilized to prevent the evaporation of the solvent. After boiling had commenced, 1 mL of $HAuCl_4$ (25 mM) was injected. The color of the solution changed from yellow to bluish gray and then, to soft pink in 10 min. Under these conditions, the resulting particles (9 ± 2 nm, ~3×10^{12} NPs/mL) were coated with negatively charged citrate ions and hence, they were well suspended in H_2O. After the Au nanoparticle solution was cooled to room temperature, a solution of 0.5 g of polyvinylpyrrolidone (PVP, MW = 40,000) in water (20 mL) was added dropwise to the Au nanoparticle solution under continuous stirring, and the mixture was further stirred at room temperature for 24 h. Then, 600 mL of acetone were added to this mixture and left overnight. The supernatant was removed, and the resulting nanoparticles were washed three times with methanol, and finally dispersed in methanol at a concentration of 0.6 mg/mL.

Synthesis of Au nanoparticles (~22 nm diameter). A solution of 2.2 mM sodium citrate in DI water (150 mL) was heated with a heating mantle in a 250 mL three-necked round-bottomed flask for 15 min under vigorous stirring. A condenser was utilized to prevent the evaporation of the solvent. After boiling had commenced, 1 mL of $HAuCl_4$ (25 mM) was injected. The color of the solution changed from yellow to bluish gray and then to soft pink in 10 min. Then, the reaction was cooled until the temperature of the solution reached 90 ºC, after that, 1 mL of a $HAuCl_4$ solution (25 mM) was injected to the solution and stirred for 30 min. This process was repeated one more time. Under these conditions, the resulting particles (22 ± 2 nm, ~1.2 x 10^{12} NPs/mL) were coated with negatively charged citrate ions and hence, they were well suspended in H_2O. After the Au nanoparticle solution was cooled to room temperature, a solution of 0.5 g PVP in water (20 mL) was added dropwise to the Au nanoparticle solution under continuous stirring, and the mixture was further stirred at room temperature for 24 h. Then, 600 mL of acetone were added to this mixture and left overnight. The supernatant was removed, and the resulting nanoparticles were washed three times with methanol, and finally dispersed in methanol at a concentration of 1.4 mg/mL.[48]

Synthesis of Au nanoparticles (~4 nm diameter). A solution of 2.2 mM sodium citrate in DI water (300 mL) was heated up to 70˚ C under vigorous stirring. Then, 0.2 mL of tannic acid (2.5 mM) and 2 mL of potassium carbonate (K_2CO_3, 150 mM) were added to the heated solution. Afterwards 2 mL of $HAuCl_4$ (25 mM) was injected, and the color of the solution changed

from yellow to bluish gray to reddish orange in 10 min. The solution was stirred at the same temperature for 2 hours. Under these conditions, the resulting nanoparticles (3.6 ± 0.4 nm, 0.2 mg/mL) were coated with negatively charged citrate ions and hence, they were well suspended in H_2O. The same coating producer as for Au nanoparticles (~9 nm diameter) was used to functionalize these nanoparticles with PVP.[49]

Synthesis of cubic Pd nanoparticles (~18 nm diameter). 547 mg of KBr, 100 mg of PVP (MW = 55,000), 51 mg of $NaPdCl_4$ and 55 mg of l-ascorbic acid were added to 10 mL of DI water and heated to 80 ˚C under reflux and vigorous stirring for 3 h. After the nanoparticle solution was cooled to room temperature, the nanoparticles were washed twice with a mixture of acetone and water and one time with methanol, and finally dispersed in methanol at a concentration of 0.5 mg/mL (size = 18 ± 2 nm).[6]

Synthesis of icosahedral Pd nanoparticles (~13 nm diameter): In a standard procedure for the synthesis of Pd icosahedra, 160 mg of PVP and 20 µl of HCL (3M) were introduced into 4 mL of diethylene glycol (DEG) hosted in a 20 mL vial. This mixture was preheated in an oil bath at 105 ˚C for 20 min under magnetic stirring. Subsequently, 2 mL of DEG solution containing 31 mg of Na_2PdCl_4 was added using a pipette. After the reaction had proceeded for 1 h, it was quenched by immersing the vial in an ice/water bath. Finally, the product was collected by centrifugation, washed once with acetone and twice with water to remove DEG and excess of PVP, and finally dispersed in methanol at a concentration of 0.6 mg/mL (size = 13 ± 4 nm).[50]

Synthesis of Cu/Pd nanoparticles (~10 nm diameter). In a typical process, 10 mg of $NaPdCl_2$, 36 mg of $CuSO_4$ and 240 mg of sodium citrate were added to a mixture of 40 mL DIwater and 20 mL ethylene glycol. This mixture was then heated in an oil bath up to 160˚ C in a 100 mL round-bottomed flask under vigorous stirring for 6 h. A condenser was utilized to prevent the evaporation of the solvent. After the nanoparticle solution was cooled to room temperature, a solution of 0.7 g PVP (MW = 55,000) in water (10 mL) was added dropwise to the nanoparticle solution under continuous stirring and the mixture was further stirred at room temperature for 24 h. Then, 200 mL of acetone were added to this mixture and left overnight. The supernatant was removed, and the resulting nanoparticles were washed twice with water and twice with methanol, and finally dispersed in methanol at a concentration of 1.8 mg/mL (size = 10 ± 3 nm, Cu:Pd = 1:2).

Synthesis of Au(9nm)-on-ZIF-67 composites. 10 mg of the $C/T/H_{ZIF\text{-}67}$ was dispersed in 5 mL of ethanol in a sonication bath for 10 min and then, 10 mL of Au nanoparticle solution was added dropwise to the dispersion while stirring. The resulting composites were collected by centrifugation, washed twice with ethanol and dried at 60 ºC overnight.

Synthesis of $tRD_{ZIF\text{-}8}$-on-Au(9nm)-on-ZIF-67 composites. The same general route for growing $tRD_{ZIF\text{-}8}$-on-$C_{ZIF\text{-}67}$ was applied. The only difference is that we used Au(9nm)-on-$C_{ZIF\text{-}67}$ cores in various shapes instead of only ZIF-67 cores.

Synthesis of $RD_{ZIF\text{-}8}$-on-INPs-on-$tRD_{ZIF\text{-}8}$-on-Au(9nm)-on-$C_{ZIF\text{-}67}$ layered composites. 10 mg of the $tRD_{ZIF\text{-}8}$-on-Au(9 nm)-on-$C_{ZIF\text{-}67}$ crystals were dispersed in 5 mL of ethanol in a sonication bath for 10 min. Then, desired amount of the corresponding INP (22 nm-in-diameter Au NPs, 13 nm-in-diameter icosahedral Pd NPs or 18 nm-in-size cubic Pd NPs) solution was added dropwise to the dispersion while stirring. The resulting composites were collected by centrifugation, washed twice with ethanol and dried at 60 ºC overnight. The different INP-on-$tRD_{ZIF\text{-}8}$-on-Au(9nm)-on-$C_{ZIF\text{-}67}$ composite crystals were finally subjected to a ZIF-8 growing using C = 10 mM and t = 1 day.

Synthesis of INP-on-$tRD_{ZIF\text{-}8}$ composites. The same general route for growing Au(9nm)-on-$C_{ZIF\text{-}67}$ was applied. 10 mg of $tRD_{ZIF\text{-}8}$ particles were dispersed in 5 mL of methanol in a sonication bath for 10 min. Then, 10 ml of Au (3 nm) nanoparticle solution, 1 ml of Cu/Pd (10 nm) nanoparticle solution or a mixture of both nanoparticle solutions were added dropwise to this dispersion under continuous stirring. The different Au-on-$tRD_{ZIF\text{-}8}$, Cu/Pd-on-$tRD_{ZIF\text{-}8}$ and Au/Cu/Pd-on-$tRD_{ZIF\text{-}8}$ composites were collected by centrifugation, washed twice with ethanol and dried at 60 ºC overnight.

Synthesis of INP-on-$tRD_{ZIF\text{-}8}$-on-INP-on-$tRD_{ZIF\text{-}8}$ layered composites. A similar methodology used for growing $RD_{ZIF\text{-}8}$-on-INPs-on-$tRD_{ZIF\text{-}8}$-on-Au(9nm)-on-$C_{ZIF\text{-}67}$ layered composites was applied. 10 mg of INP-on-$tRD_{ZIF\text{-}8}$ particles were dispersed in 10 mL of methanol in a sonication bath for 10 min. Then, 5 mL of 25 mM 2-MiM and 5 mL of 25 mM $Zn(NO_3)_2.6H_2O$ in methanol were sequentially added to this dispersion in this order, and left at room temperature without stirring for 10 min. The resulting particles were collected by centrifugation, washed twice with methanol and dried at 60 ºC overnight. Then, 10 mg of these particles were dispersed in 5 mL of methanol in a sonication bath for 10 min. Afterwards, desired amount of the corresponding INP (Au (3 nm) or Cu/Pd (10 nm)) solution was added dropwise to the dispersion under continuous stirring. The final particles were collected by centrifugation, washed once with methanol and dried at 60 ºC overnight.

General route for the catalytic reactions. A mixture of 1-(prop-2-yn-1-yloxy)naphthalene (**1**) (2.32 mg, 12.7 µmol), K_2CO_3 (3.52 mg, 25.5 µmol), iodobenzene (PhI) (1.42 µL, 12.7 µmol), Xantphos (0.37 mg, 0.63 µmol), mesitylene as internal standard (0.35 µL, 5.1 µmol) and the desired ZIF-8-based catalyst (5 mol%) were mixed in 0.6 mL of dry toluene, in a 2 mL sealed vial. The dispersion was sonicated for 15 min and stirred for 6 days at 110 ºC. Afterwards, the raw solution was filtered through a silica pad, and 4 mL of ethyl acetate were passed to eluate all the generated products. The obtained components were analyzed and quantified by means of Gas Chromatography and ^{1}H-NMR (see Table 1). Compounds **1**, **2**, **3** and **4** were synthesized and characterized according to the literature.[51-55]

Characterization. Powder X-ray diffraction (PXRD) patterns were collected on an X'Pert PRO MPDP analytical diffractometer (Panalytical) at 45 kV, 40 mA using Cu Kα radiation (λ=1.5419Å). Nitrogen adsorption and desorption measurements were done at 77˚ K using an Autosorb-IQ-AG analyser (Quantachrome Instruments). Field-Emission Scanning Electron Microscopy (FE-SEM) images were collected on a FEI Magellan 400L scanning electron microscope at an acceleration voltage of 1.0–2.0 kV, using aluminum as support. High-angle annular dark-field scanning transmitted electron microscopy (HAADF-STEM) images were obtained with a FEI Tecnai G2 F20 at 200 kV. Metal contents of all composites were determined by Inductively Coupled Plasma – Optical Emission Spectroscopy (ICP-OES). These measurements were performed using an ICP-OES Perkin-Elmer, model Optima 4300DV previous digestion of the composites in a mixture of HNO_3 and HCl

(1:2) at 220 ºC. Gas chromatography product analyses were performed on an Agilent 7820A gas chromatograph equipped with a HP-5 capillary column (30 m x 0.32 mm x 0.25μm). The injection was carried out on a split/splitless automatic injector Agilent G4513A, in split mode with ratio 100:1 with an injected volume of 1μL. The detection was conducted by a flame ionization detector (Agilent 7820A GC-System). ^{1}H-NMR data concerning product identity were collected with a Bruker 400 AVANCE (Serveis Tècnics de Recerca, University of Girona) spectrometer in the corresponding deuterated solvent ($CDCl_3$) and calibrated relative to the residual protons of the solvent. 1,3,5-trimethoxybenzene (mesitylene) was used as internal standard.

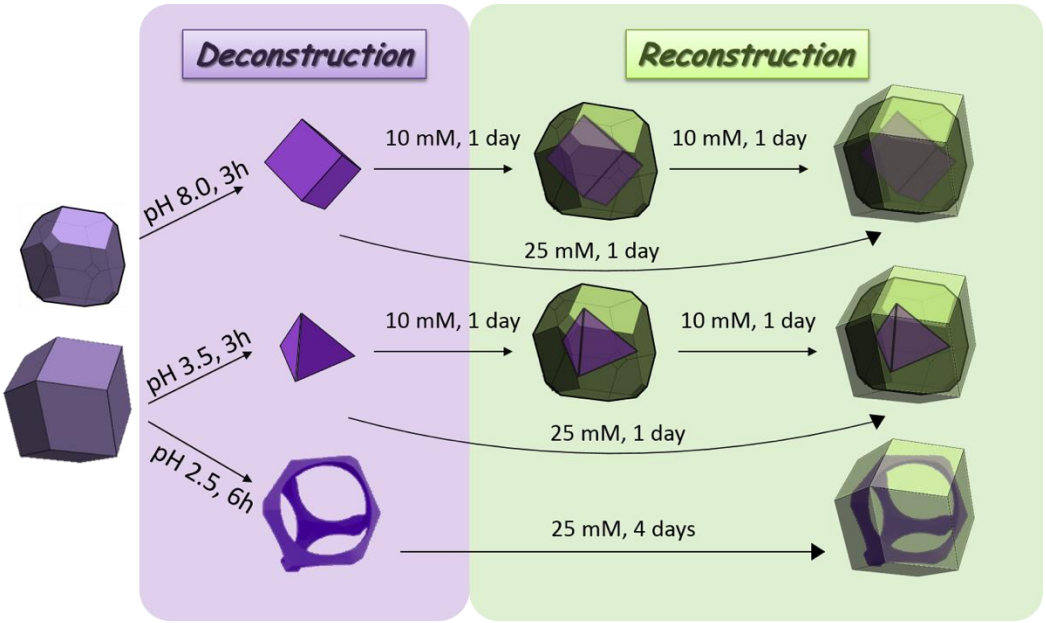

Figure 1. Schematic illustration of the synthetic conditions used to construct the different ZIF-8-on-ZIF-67 particles according to the sequential deconstruction-reconstruction strategy.

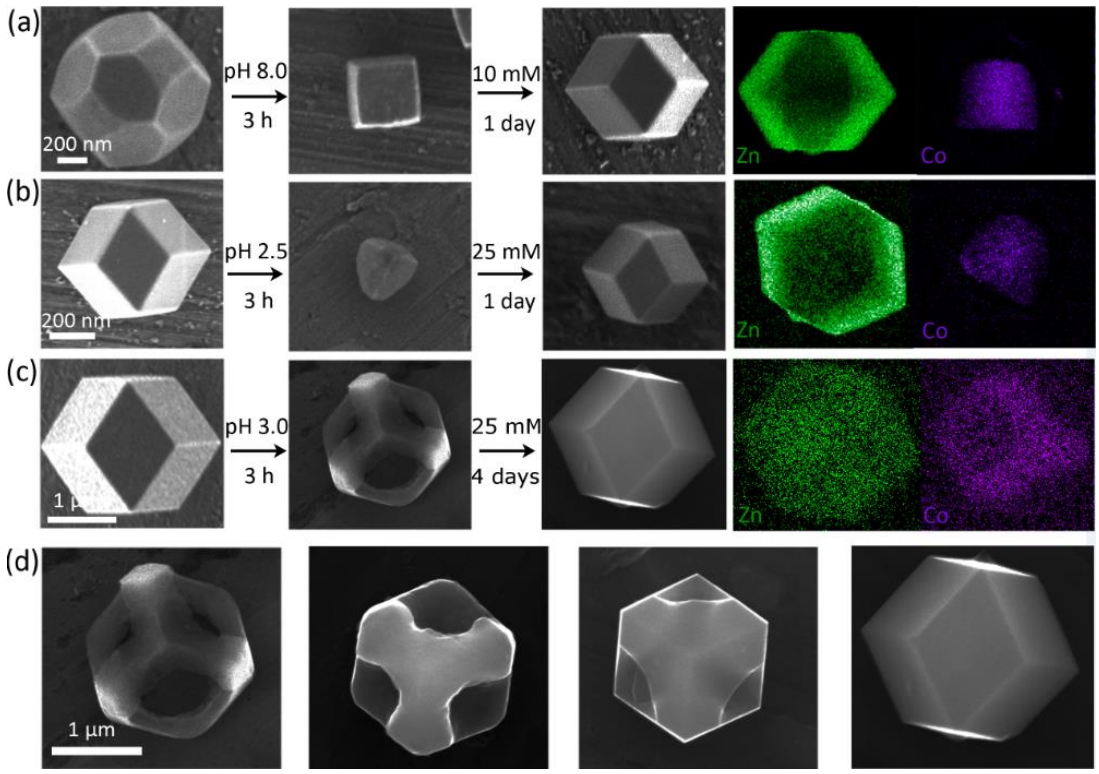

Figure 2. (a-c) FE-SEM images of single particles showing the formation of $RD_{ZIF\text{-}8}$-on-$C_{ZIF\text{-}67}$ (a), $RD_{ZIF\text{-}8}$-on-$T_{ZIF\text{-}67}$ (b) and $RD_{ZIF\text{-}8}$-on-$H_{ZIF\text{-}67}$ (c) particles built by the deconstruction-reconstruction strategy. Right-hand panel: the corresponding elemental mapping (EDX) results, showing the distribution of Zn (green) and Co (violet). (d) FE-SEM images showing the evolution of the formation of $RD_{ZIF\text{-}8}$-on-$H_{ZIF\text{-}67}$.

RESULTS AND DISCUSSION

Figure 1 depicts the different ZIF-8-on-ZIF-67 particles generated by sequential deconstruction-reconstruction. This process starts with anisotropic etching of the ZIF-67 particles to C, H and T particles under our previously reported synthetic conditions.[27] The resulting etched particles are then dispersed in methanol (MeOH) and mixed with a solution of 2-methylimidazole (2-MiM) in MeOH at an optimized concentration. Afterwards, a solution of $Zn(NO_3)_2 \cdot 6H_2O$ in MeOH at the same concentration is added, and the resulting mixture is left at room temperature for a certain time. Note that the required precursor concentration and the reaction time vary by the initial morphology of the etched core particle and that, in all cases, we could optimize them to selectively generate tRD or RD particles. For instance, when the core was a cubic or tetrahedral ZIF-67 particle, $tRD_{ZIF\text{-}8}$-on-$C_{ZIF\text{-}67}$ and $tRD_{ZIF\text{-}8}$-on-$T_{ZIF\text{-}67}$ particles were formed at a concentration of 10 mM and a reaction time of 1 day. In contrast, $RD_{ZIF\text{-}8}$-on-$C_{ZIF\text{-}67}$ and $RD_{ZIF\text{-}8}$-on-$T_{ZIF\text{-}67}$ particles were synthesized by increasing the concentration up to 25 mM and maintaining the reaction time at 1 day (for full synthetic procedures, see experimental section).

For the hollow microboxes, $RD_{ZIF\text{-}8}$-on-$H_{ZIF\text{-}67}$ particles were formed at a concentration of 25 mM and a reaction time of 4 days. With this core, controlled growth of an external $tRD_{ZIF\text{-}8}$ layer was not possible, since in etched hollow microboxes all six (100) vertices are already fully grown. However, the RD shape was fully recovered. Indeed, we found that these particles grew mainly inside of the hollow core, thus fully reversing the etching process (Figure 2d).

Comparison of Field-Emission Scanning Electron Microscope (FE-SEM) images of the etched particles and the resulting ZIF-8-on-ZIF-67 particles confirmed their reconstruction into homogeneous tRD or RD particles (Figure 2 and S1). The internal composition of single particles was investigated by elemental mapping with energy dispersive X-ray spectrometry (EDX), which revealed a distribution of Co atoms following the shape of the initial etched ZIF-67 particles and a distribution of Zn atoms corresponding to the newly reconstructed layers (Figure 2). Moreover, PXRD patterns and BET surface areas ($RD_{ZIF\text{-}8}$-on-$C_{ZIF\text{-}67}$, S_{BET} = 1417 m^2/g; $RD_{ZIF\text{-}8}$-on-$T_{ZIF\text{-}67}$, S_{BET} = 1422 m^2/g; and $RD_{ZIF\text{-}8}$-on-$H_{ZIF\text{-}67}$, S_{BET} = 1324 m^2/g) confirmed that these ZIF-on-ZIF systems are pure ZIF-8/ZIF-67 (Figure S3 and S4). Also note here that all $RD_{ZIF\text{-}8}$-on-$(C/T)_{ZIF\text{-}67}$ particles could be generated from the $tRD_{ZIF\text{-}8}$-on-$(C/T)_{ZIF\text{-}67}$ particles under the conditions described in Figure 1.

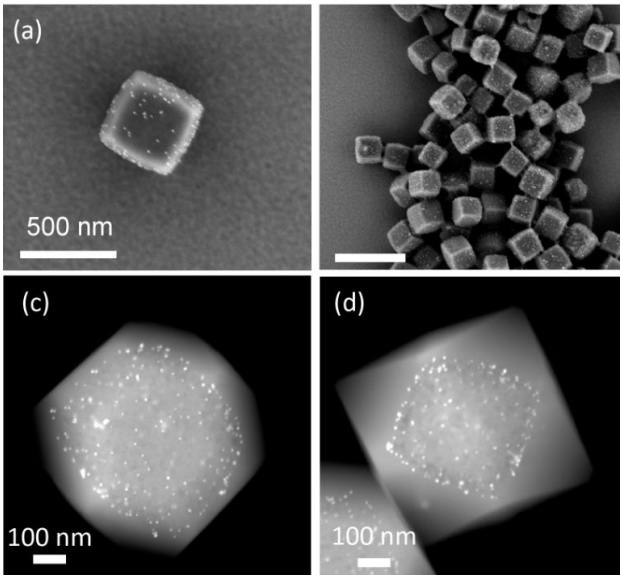

Figure 3. (a,b) FE-SEM images showing an individual (a) and a general view (b) of Au(9nm)-on-$C_{ZIF\text{-}67}$ composites. (c,d) HAADF-STEM images of single $tRD_{ZIF\text{-}8}$-on-Au(9nm)-on-$C_{ZIF\text{-}67}$ (c) and $RD_{ZIF\text{-}8}$-on-Au(9nm)-on-$C_{ZIF\text{-}67}$ (d) composites.

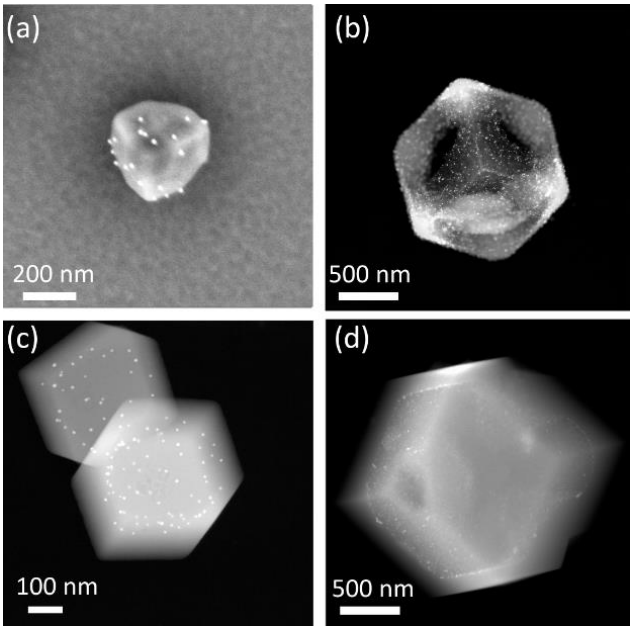

Figure 4. (a) FE-SEM image showing an individual Au-on-$T_{ZIF\text{-}67}$ composite. (b) HAADF-STEM image of a single Au-on-$H_{ZIF\text{-}67}$ composite. (c,d) HAADF-STEM images of single $RD_{ZIF\text{-}8}$-on-Au-on-$T_{ZIF\text{-}67}$ (c) and $RD_{ZIF\text{-}8}$-on-Au-on-$H_{ZIF\text{-}67}$ (d) composites.

Altogether these experiments showed that, even for the hollow microboxes, all etched cores can be reconstructed to its original shape by controlled re-growing. The fact that all the final shapes are similarly {110} dominant is the consequence of the difference in the growing kinetics in the <100>, <110> and <111> directions, from which <110> is the slowest.

Having demonstrated that stepwise reconstruction of our etched particles from C/T to tRD to RD was possible, we envisioned using our strategy to make layered ZIF-8-on-INP-on-ZIF-67 composites by simply attaching the INPs onto the crystal surfaces of the etched ZIF-67 particles before their reconstruction. To this end, we began by investigating attachment of Au NPs (~ 9 nm diameter) to the crystal surface of C particles of ZIF-67. The formed Au NPs were previously coated with polyvinylpyrrolidone (PVP; see Supporting Information), and then quantitatively attached to the ZIF-67 particles by simply adding them dropwise to a colloidal solution of ZIF-67 particles in MeOH (5 mg/mL) under vigorous stirring. After 1 min, Au(9nm)-on-$C_{ZIF\text{-}67}$ composites and a transparent supernatant were separated by centrifugation. Remarkably, the transparency of the supernatant indicated that it was deprived of Au NPs, and therefore, that the Au NPs had attached to the ZIF-67 particles massively. Indeed, FE-SEM images of the Au(9nm)-on-$C_{ZIF\text{-}67}$ composites revealed homogeneous attachment of the Au NPs to the crystal surface of ZIF-67 and did not show any evidence of

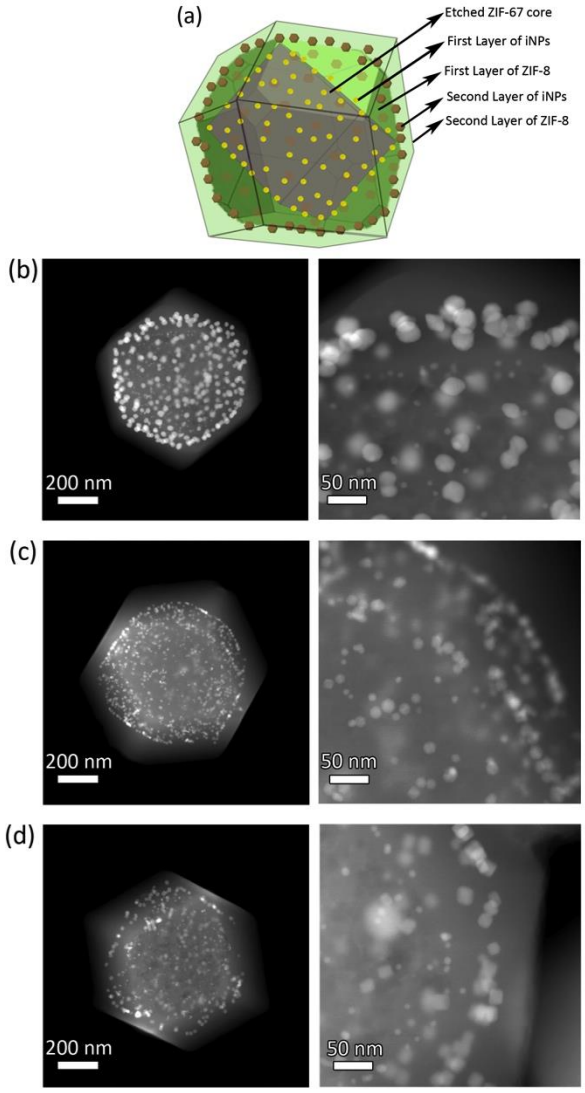

Figure 5. (a) Schematic illustration of the ZIF-based composites composed of two different layers of INPs. (b-d) HAADF-STEM images of single $RD_{ZIF\text{-}8}$-on-Au(22 nm)-on-$tRD_{ZIF\text{-}8}$-on-Au(9nm)-on-$C_{ZIF\text{-}67}$ (b), $RD_{ZIF\text{-}8}$-on-Pd(icosahedral)-on-$tRD_{ZIF\text{-}8}$-on-Au(9nm)-on-$C_{ZIF\text{-}67}$ (c), and $RD_{ZIF\text{-}8}$-on-Pd(cubic)-on-$tRD_{ZIF\text{-}8}$-on-Au(9nm)-on-$C_{ZIF\text{-}67}$ (d) composites.

significant Au-Au aggregation, neither presence of isolated Au NPs in the background (Figures 3a,b).

We then attempted to grow a ZIF-8 layer on top of the Au(9nm)-on-$C_{ZIF\text{-}67}$ composites, seeking to control the reconstruction into either tRD or RD shapes. Thus, we reproduced the same growing conditions as for $C_{ZIF\text{-}67}$ except that we used a dispersion of Au-on-$C_{ZIF\text{-}67}$ in MeOH (5 mg/mL). Figures 3c,d show that, when a solution of 2-MiM/$Zn(NO_3)_2{\cdot}6H_2O$ was used at concentrations of 10 mM or 25 mM, $tRD_{ZIF\text{-}8}$-on-Au(9nm)-on-$C_{ZIF\text{-}67}$ or $RD_{ZIF\text{-}8}$-on-Au(9nm)-on-$C_{ZIF\text{-}67}$ composites, respectively, were formed. Remarkably, we could apply the same sequential process for the T and H particles, enabling us to generate the corresponding $RD_{ZIF\text{-}8}$-on-Au(9nm)-on-$T_{ZIF\text{-}67}$ and $RD_{ZIF\text{-}8}$-on-Au(9nm)-on-$H_{ZIF\text{-}67}$ particles (Figure 4). The homogeneity of the Au NP distribution observed in Figures 3 and 4 witnesses the ordered formation of the growing ZIF-8 layer in the experimental conditions

Having shown that the layer of Au NPs does not preclude ZIF reconstruction and that reconstruction could be done stepwise, we next sought to use our strategy to construct onion-like composites made of (multi)-layered INPs (Figure 5a). To do this, we divided the $tRD_{ZIF\text{-}8}$-on-Au(9nm)-on-$C_{ZIF\text{-}67}$ particles into three portions, to each of which we attached either PVP-coated Au NPs (~22 nm in diameter), icosahedral Pd NPs (~13 nm in diameter) or cubic Pd NPs (~18 nm in side length), using the same protocol. Then, similarly to in the first reconstruction process, we deposited a second ZIF-8 layer using a precursor concentration of 10 mM and a reaction time of 1 day. Figure 5b-d and Figure S5 show High Angle Annular Dark Field Scanning Transmission Electron Microscopy (HAADF-STEM) images of three resulting multi-composites, revealing RD as the final shape and two different layers of INPs: that is, an internal layer of Au NPs (9 nm) and an external layer of either Au NPs (22 nm), icosahedral Pd NPs (13 nm) or cubic Pd NPs (18 nm). These (multi)-layered composites were found to retain the crystallinity and porosity of the starting ZIF particles (Figures S6 and S7). Interestingly, the two different layers of INPs inside a single ZIF particle could be separated by a distance of 40-50 nm (Figure 5b-d, right column).

MOF particles composed of separated layers of INPs should be useful for heterogeneous cascade catalysis because the involved reactions can be chronologically catalyzed in a stepwise manner. As a proof-of-concept, we studied a cascade reaction comprising a first Sonogashira coupling from 1-(prop-2-yn-1-yloxy)naphthalene (**1**) to 1-((3-phenylprop-2-yn-1-yl)oxy)naphthalene (**2**) catalyzed by Cu/Pd NPs, followed by a second cyclization reaction from **2** to 4-phenyl-2H-benzo[h]chromene (**3**) catalyzed by Au NPs (Figure 6a). We selected this reaction because the cyclization of **1** to 2H-benzo[h]chromene (**4**) can occur either under thermal conditions,[56] or can be catalyzed by Au NPs, thus highlighting the importance of the INP that starts catalyzing the reaction involving **1**.

Accordingly, we synthesized a composite composed of an internal layer of Au NPs (~4 nm in diameter) and an external layer of Cu/Pd NPs (~10 nm in diameter) (Figure 6b). In this composite, both core and layer separating the INPs was ZIF-8 because it is more stable than ZIF-67. The thickness of the ZIF-8 layer was as small as 20 nm to facilitate the diffusion of the large reagents that occurs mainly through the framework and/or layer defects (Figure 6c).[57] The catalytic cascade reactions were then conducted by mixing **1**, K_2CO_3, iodobenzene (PhI) and Xantphos in toluene with a toluene dispersion of Cu/Pd-on-$tRD_{ZIF\text{-}8}$-on-Au-on-$tRD_{ZIF\text{-}8}$ (Au: 2.2% w/w; Cu: 0.6% w/w; Pd: 1.3% w/w; metal content was estimated by analyzing the digested composite by ICP-OES), and reacted at 110 ºC for 6 days under continuous stirring. As control experiments, we also reproduced the same reaction using $tRD_{ZIF\text{-}8}$ (without NPs), Au-on-$tRD_{ZIF\text{-}8}$ (Au: 2.1% w/w), Cu/Pd-on-$tRD_{ZIF\text{-}8}$ (Cu: 0.6 % w/w; Pd: 1.2% w/w), Au-on-$tRD_{ZIF\text{-}8}$-on-Cu/Pd-on-$tRD_{ZIF\text{-}8}$ (Au: 2.2% w/w; Cu: 0.5% w/w; Pd: 1.0% w/w) and Au/Cu/Pd-on-$tRD_{ZIF\text{-}8}$ (Au: 2.1% w/w; Cu: 0.5% w/w; Pd: 1.2% w/w) as catalysts (Table 1).

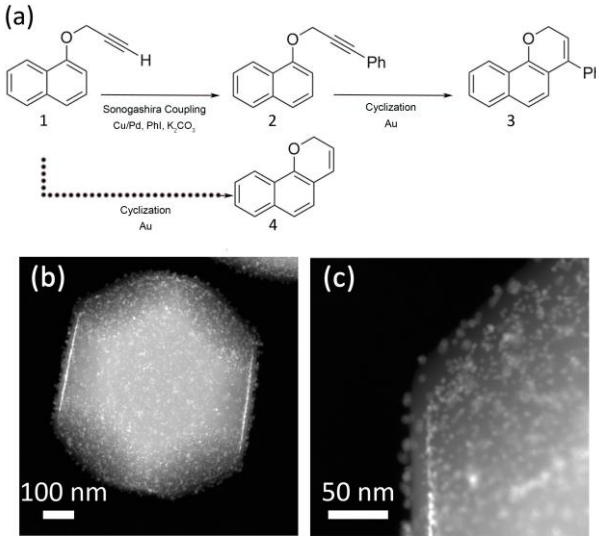

Figure 6. (a) Schematic illustration of the cascade reaction. (b-c) HAADF-STEM images of Cu/Pd-on-tRD$_{ZIF-8}$-on-Au-on-tRD$_{ZIF-8}$ composite.

In the case of ZIF-8 and the composite containing only Au NPs, Au-on-tRD$_{ZIF-8,}$ they produced the non-desired **4** (yield: 21 and 31%, respectively) (see Figure 6a). The 21 % of **4** produced using only ZIF-8 was exclusively due to the thermal conditions of the reaction, as seen from blanks in Table 1 (entries 1 and 9). Note also here that a higher yield of **4** (65 %) was obtained when Au-on-tRD$_{ZIF-8}$ was used without K_2CO_3. This yield increase demonstrates that K_2CO_3, which is necessary for the Sonogashira coupling, is detrimental for the cyclization reaction. For the composite containing only Cu/Pd NPs, Cu/Pd-on-tRD$_{ZIF-8}$, a mixture of **2** (yield: 35 %) and **4** (yield: 8 %) was synthesized. For the (multi)-layered composite with the incorrect sequence of INPs (external: Au NPs; internal: Cu/Pd NPs), it also produced **4** (yield: 18%), and not **2** or **3**, proving that the cyclization of **1** mainly takes place as it first encounters Au NPs and not Cu/Pd NPs, which were embedded further in the ZIF. For the composite that contains a mixture of both types of NPs on the external surface, Au/Cu/Pd-on-tRD$_{ZIF-8}$, **2** was mainly produced (yield: 28 %). In this reaction, small proportions of **3** (yield: 4 %) resulting from the cascade reaction and **4** (yield: 2%) were also formed. For the composite with the good sequence, Cu/Pd-on-RD$_{ZIF-8}$-on-Au-on-tRD$_{ZIF-8}$, we mainly obtained **2** (yield: 53 %), a higher proportion of **3** (yield: 11 %) and a small proportion of **4** (1 %). The increase in the formation of **3** agrees with the occurrence of the cascade reaction, which is first catalyzed with Cu/Pd NPs and then with Au NPs. In addition, the yield of **3** also agrees with the expected value taking into account the independent performance of both reactions involved in the cascade process (Figure 6a). Indeed, as seen before, reaction of **1** in the presence of Cu/Pd-on-tRD$_{ZIF-8}$ gave **2** (yield: 35 %), whereas the reaction of **2** in the presence of Au-on-tRD$_{ZIF-8}$ gave **3** (yield: 22 %). These values result in an expected yield for the cascade reaction of 8 %. Nevertheless, the fact that a higher yield of **3** could be obtained using Cu/Pd-on-tRD$_{ZIF-8}$-on-Au-on-tRD$_{ZIF-8}$ in comparison to the other binary Au-on-tRD$_{ZIF-8}$-on-Cu/Pd-on-tRD$_{ZIF-8}$ and Au/Cu/Pd-on-tRD$_{ZIF-8}$ composites is a first proof-of-concept that (multi)-layered MOF composites with a suitable sequence of INPs can potentially catalyze cascade reactions.

Table 1. Summary of the catalytic reactions.

Entry	Catalyst	1 (%)	2 (%)	3 (%)	4 (%
1[a]	ZIF-8	58	-	-	2
2[a]	Au-on-tRD$_{ZIF-8}$	40	-	-	3
3[a,b,c]	Au-on-tRD$_{ZIF-8}$ (reaction from **2** to **3**)	-	64	22	-
4	Cu/Pd-on-tRD$_{ZIF-8}$	20	35	-	8
5	Cu/Pd-on-tRD$_{ZIF-8}$-on-Au-on-tRD$_{ZIF-8}$	-	53	11	1
6	Au-on-tRD$_{ZIF-8}$-on-Cu/Pd-on-tRD$_{ZIF-8}$	45	-	-	1
7	Au/Cu/Pd-on-tRD$_{ZIF-8}$	-	28	4	2
9[a]	No ZIF-8	53	-	-	1
10[b]	ZIF-8	-	71	8	-
11[b]	No ZIF-8	-	71	11	-

[a] Without PhI and Xantphos.
[b] 2 as starting material.
[c] 3 days.

CONCLUSIONS

In conclusion, we have reported that ZIF-8/ZIF-67 particles that have been etched can be fully reconstructed, and that this reversibility can be used as an alternative strategy to synthesize novel ZIF-on-ZIF and layered ZIF-on-INP-on-ZIF composites. The first step of our approach comprises anisotropic etching of ZIF-8/ZIF-67 particles, which yields unprecedented C, T and H morphologies. Secondly, exposing these etched particles to a ZIF precursor solution enables their reversible construction. Here, precursor concentration and regrowth time were critical variables for optimizing the final shape (tRD or RD) of the reconstructed particles. Moreover, we have demonstrated that even hollow microboxes can be recovered to a final RD shape by filling the inner space of the box with ZIF-8. Remarkably, the reconstruction step may also be accompanied with a step for attaching PVP-capped INPs onto the ZIF particle surface. This attachment, coupled with the ZIF-on-ZIF growth, affords layered ZIF-on-INP-on-ZIF composites. Furthermore, this latter process can be repeated to construct (multi)-layered composites composed of several types of INPs. In these composites, the different INPs are well separated by a nanometric layer of ZIF-8 that can be as small as 20 nm. These composites offer potential for diverse practical domains such as catalysis, among other applications. Preliminary results obtained for a model cascade reaction paves the way to an improved design of new catalytic protocols for cascade reactions.

ASSOCIATED CONTENT

Supporting Information

The Supporting Information is available free of charge on the ACS Publications website. Additional FESEM and HAADF-STEM images, PXRD, and sorption isotherms (PDF)

AUTHOR INFORMATION

Corresponding Author

* E-mail: daniel.maspoch@icn2.cat

Notes

The authors declare no competing financial interest.

ACKNOWLEDGMENT

This work was supported by the EU FP7 ERC-Co 615954, the Spanish MINECO (projects PN MAT2015-65354-C2-1-R, MAT2015-70725-R and CTQ2016-77989-P), and the Catalan AGAUR (projects 2014 SGR 80, 2014 SGR 612 and 2014 SGR 862). It was also funded by the CERCA Program/Generalitat de Catalunya. N.G.B. acknowledges financial support by MINECO through the Ramon y Cajal program (RYC-2012- 10991). ICN2 acknowledges the support of the Spanish MINECO through the Severo Ochoa Centers of Excellence Program and project MAT2016-77608-C3-1-P, under Grant SEV-2013-0295. X.R. is also grateful for ICREA-Acadèmia awards. We thank STR UdG for technical support.

REFERENCES

1. Lee, S. Y.; Gradon, L.; Janeczko, S.; Iskandar, F.; Okuyama, K., Formation of Highly Ordered Nanostructures by Drying Micrometer Colloidal Droplets. *ACS Nano* **2010,** *4*, 4717-4724.
2. Meyer, R. A.; Green, J. J. Shaping the future of nanomedicine: anisotropy in polymeric nanoparticle design. *Wiley Interdiscip. Rev.: Nanomed. Nanobiotechnol.* **2016,** *8*, 191-207.
3. Zeng, J.; Zhang, Q.; Chen, J.; Xia, Y. A comparison study of the catalytic properties of Au-based nanocages, nanoboxes, and nanoparticles. *Nano Lett.* **2010,** *10*, 30-35.
4. Chen, J.; Wiley, B.; McLellan, J.; Xiong, Y.; Li, Z.-Y.; Xia, Y. Optical Properties of Pd−Ag and Pt−Ag Nanoboxes Synthesized via Galvanic Replacement Reactions. *Nano Lett.* **2005,** *5*, 2058-2062.
5. Merkel, T. J.; Herlihy, K. P.; Nunes, J.; Orgel, R. M.; Rolland, J. P.; DeSimone, J. M. Scalable, Shape-specific, Top-down Fabrication Methods for the Synthesis of Engineered Colloidal Particles. *Langmuir* **2010,** *26*, 13086-13096.
6. Lim, B.; Jiang, M.; Tao, J.; Camargo, P. H. C.; Zhu, Y.; Xia, Y. Shape-Controlled Synthesis of Pd Nanocrystals in Aqueous Solutions. *Adv. Funct. Mater.* **2009,** *19*, 189-200.
7. Moon, S. Y.; Kusunose, T.; Sekino, T. CTAB-Assisted Synthesis of Size- and Shape-Controlled Gold Nanoparticles in SDS Aqueous Solution. *Mater. Lett.* **2009,** *63*, 2038-2040.
8. Gómez-Graña, S.; Goris, B.; Altantzis, T.; Fernández-López, C.; Carbó-Argibay, E.; Guerrero-Martínez, A.; Almora-Barrios, N.; López, N.; Pastoriza-Santos, I.; Pérez-Juste, J.; Bals, S.; Van Tendeloo, G.; Liz-Marzán, L. M. Au@Ag Nanoparticles: Halides Stabilize {100} Facets. *J. Phys. Chem. Lett.* **2013,** *4*, 2209-2216.
9. Chen, C.; Hirdes, D.; Folch, A. Gray-scale photolithography using microfluidic photomasks. *Proc. Natl. Acad. Sci. U. S. A.* **2003,** *100*, 1499-1504.
10. Liu, M.; Zheng, Y.; Zhang, L.; Guo, L.; Xia, Y. Transformation of Pd Nanocubes into Octahedra with Controlled Sizes by Maneuvering the Rates of Etching and Regrowth. *J. Am. Chem. Soc.* **2013,** *135*, 11752-11755.
11. Wang, Z.; Wang, H.; Zhang, Z.; Yang, G.; He, T.; Yin, Y.; Jin, M. Synthesis of Pd Nanoframes by Excavating Solid Nanocrystals for Enhanced Catalytic Properties. *ACS Nano* **2017,** *11*, 163-170.
12. Du, J.-H.; Sheng, T.; Xiao, C.; Tian, N.; Xiao, J.; Xie, A.-Y.; Liu, S.; Zhou, Z.-Y.; Sun, S.-G. Shape Transformation of {hk0}-Faceted Pt Nanocrystals from a Tetrahexahedron into a Truncated Ditetragonal Prism. *Chem. Commun.* **2017,** *53*, 3236-3238.
13. Lee, J. H.; Gibson, K. J.; Chen, G.; Weizmann, Y. Bipyramid-Templated Synthesis of Monodisperse Anisotropic Gold Nanocrystals. *Nat. Commun.* **2015,** *6*, 7571.
14. Choi, S.; Kim, T.; Ji, H.; Lee, H. J.; Oh, M. Isotropic and Anisotropic Growth of Metal-Organic Framework (MOF) on MOF: Logical Inference on MOF Structure Based on Growth Behavior and Morphological Feature. *J. Am. Chem. Soc.* **2016,** *138*, 14434-14440.
15. Furukawa, S.; Hirai, K.; Takashima, Y.; Nakagawa, K.; Kondo, M.; Tsuruoka, T.; Sakata, O.; Kitagawa, S. A Block PCP Crystal: Anisotropic Hybridization of Porous Coordination Polymers by Face-selective Epitaxial Growth. *Chem. Commun.* **2009**, 5097-5099.
16. Koh, K.; Wong-Foy, A. G.; Matzger, A. J. MOF@MOF: Microporous Core-Shell Architectures. *Chem. Commun.* **2009**, 6162-6164.
17. Zhao, M.; Yuan, K.; Wang, Y.; Li, G.; Guo, J.; Gu, L.; Hu, W.; Zhao, H.; Tang, Z. Metal–Organic Frameworks as Selectivity Regulators for Hydrogenation Reactions. *Nature* **2016,** *539*, 76-80.
18. Falcaro, P.; Ricco, R.; Yazdi, A.; Imaz, I.; Furukawa, S.; Maspoch, D.; Ameloot, R.; Evans, J. D.; Doonan, C. J. Application of Metal and Metal Oxide Nanoparticles@MOFs. *Coord. Chem. Rev.* **2016,** *307*, 237-254.
19. Kim, C. R.; Uemura, T.; Kitagawa, S. Inorganic Nanoparticles in Porous Coordination Polymers. *Chem. Soc. Rev.* **2016,** *45*, 3828-3845.
20. Cai, W.; Chu, C.-C.; Liu, G.; Wáng, Y.-X. J. Metal–Organic Framework-Based Nanomedicine Platforms for Drug Delivery and Molecular Imaging. *Small* **2015,** *11*, 4806-4822.
21. Doonan, C.; Riccò, R.; Liang, K.; Bradshaw, D.; Falcaro, P. Metal–Organic Frameworks at the Biointerface: Synthetic Strategies and Applications. *Acc. Chem. Res.* **2017**, *50*, 1423–1432.
22. Horcajada, P.; Chalati, T.; Serre, C.; Gillet, B.; Sebrie, C.; Baati, T.; Eubank, J. F.; Heurtaux, D.; Clayette, P.; Kreuz, C.; Chang, J.-S.; Hwang, Y. K.; Marsaud, V.; Bories, P.-N.; Cynober, L.; Gil, S.; Ferey, G.; Couvreur, P.; Gref, R. Porous Metal-Organic-Framework Nanoscale Carriers as a Potential Platform for Drug Delivery and Imaging. *Nat. Mater.* **2010**, *9*, 172-178.
23. Li, Z.; Zeng, H. C. Surface and Bulk Integrations of Single-Layered Au or Ag Nanoparticles onto Designated Crystal Planes {110} or {100} of ZIF-8. *Chem. Mater.* **2013**, *25*, 1761-1768.
24. Hu, Z.; Zhang, Z.; Li, Z.; Dou, M.; Wang, F. One-Step Conversion from Core–Shell Metal–Organic Framework Materials to Cobalt and Nitrogen Codoped Carbon Nanopolyhedra with Hierarchically Porous Structure for Highly Efficient Oxygen Reduction. *ACS Appl. Mater. Interfaces* **2017**, *9*, 16109-16116.
25. Zhang, J.; Zhang, T.; Xiao, K.; Cheng, S.; Qian, G.; Wang, Y.; Feng, Y. Novel and Facile Strategy for Controllable Synthesis of Multilayered Core–Shell Zeolitic Imidazolate Frameworks. *Cryst. Growth Des.* **2016,** *16*, 6494-6498.
26. Tang, J.; Salunkhe, R. R.; Liu, J.; Torad, N. L.; Imura, M.; Furukawa, S.; Yamauchi, Y. Thermal Conversion of Core-Shell Metal-Organic Frameworks: a New Method for Selectively

Functionalized Nanoporous Hybrid Carbon. *J. Am. Chem. Soc.* **2015,** *137*, 1572-1580.
27. Avci, C.; Ariñez-Soriano, J.; Carné-Sánchez, A.; Guillerm, V.; Carbonell, C.; Imaz, I.; Maspoch, D. Post-synthetic Anisotropic Wet-Chemical Etching of Colloidal Sodalite ZIF Crystals. *Angew. Chem. Int. Ed.* **2015,** *54*, 14417-14421.
28. Pang, S. H.; Han, C.; Sholl, D. S.; Jones, C. W.; Lively, R. P. Facet-Specific Stability of ZIF-8 in the Presence of Acid Gases Dissolved in Aqueous Solutions. *Chem. Mater.* **2016,** *28*, 6960-6967.
29. Liu, W.; Huang, J.; Yang, Q.; Wang, S.; Sun, X.; Zhang, W.; Liu, J.; Huo, F. Multi-shelled Hollow Metal–Organic Frameworks. *Angew. Chem. Int. Ed.* **2017**, *56*, 5512-5516.
30. Hu, M.; Ju, Y.; Liang, K.; Suma, T.; Cui, J.; Caruso, F. Void Engineering in Metal-Organic Frameworks via Synergistic Etching and Surface Functionalization. *Adv. Funct. Mater.* **2016,** *26*, 5827-5834.
31. Chou, L.-Y.; Hu, P.; Zhuang, J.; Morabito, J. V.; Ng, K. C.; Kao, Y.-C.; Wang, S.-C.; Shieh, F.-K.; Kuo, C.-H.; Tsung, C.-K. Formation of Hollow and Mesoporous Structures in Single-Crystalline Microcrystals of Metal-Organic Frameworks via Double-solvent Mediated Overgrowth. *Nanoscale* **2015,** *7*, 19408-19412.
32. Chen, H.; Shen, K.; Chen, J.; Chen, X.; Li, Y. Hollow-ZIF-Templated Formation of a ZnO@C–N–Co Core–Shell Nanostructure for Highly Efficient Pollutant Photodegradation. *J. Mater. Chem. A* **2017,** *5*, 9937-9945.
33. Jiang, Z.; Li, Z.; Qin, Z.; Sun, H.; Jiao, X.; Chen, D. LDH Nanocages Synthesized with MOF Templates and their High Performance as Supercapacitors. *Nanoscale* **2013,** *5*, 11770-11775.
34. Zhang, P.; Guan, B. Y.; Yu, L.; Lou, X. W. D. Formation of Double-Shelled Zinc-Cobalt Sulfide Dodecahedral Cages from Bimetallic Zeolitic Imidazolate Frameworks for Hybrid Supercapacitors. *Angew. Chem. Int. Ed.* **2017,** *56*, 7141-7145.
35. Li, S.; Dharmarwardana, M.; Welch, R. P.; Ren, Y.; Thompson, C. M.; Smaldone, R. A.; Gassensmith, J. J. Template-Directed Synthesis of Porous and Protective Core-Shell Bionanoparticles. *Angew. Chem. Int. Ed.* **2016,** *55*, 10691-10696.
36. Lu, G.; Li, S.; Guo, Z.; Farha, O. K.; Hauser, B. G.; Qi, X.; Wang, Y.; Wang, X.; Han, S.; Liu, X.; DuChene, J. S.; Zhang, H.; Zhang, Q.; Chen, X.; Ma, J.; Loo, S. C.; Wei, W. D.; Yang, Y.; Hupp, J. T.; Huo, F. Imparting Functionality to a Metal-Organic Framework Material by Controlled Nanoparticle Encapsulation. *Nat. Chem.* **2012,** *4*, 310-316.
37. Yazdi, A.; Mercoci, F.; Bastus, N. G.; Imaz, I.; Puntes, V.; Maspoch, D. The Influence of the MOF Shell Thickness on the Catalytic Performance of Composites made of Inorganic (Hollow) Nanoparticles Encapsulated into MOFs. *Catal. Sci. Technol.* **2016,** *6*, 8388-8391.
38. Liang, K.; Ricco, R.; Doherty, C. M.; Styles, M. J.; Bell, S.; Kirby, N.; Mudie, S.; Haylock, D.; Hill, A. J.; Doonan, C. J.; Falcaro, P. Biomimetic Mineralization of Metal-Organic Frameworks as Protective Coatings for Biomacromolecules. *Nat. Commun.* **2015**, *6*, 7240.
39. Jiang, H.-L.; Liu, B.; Akita, T.; Haruta, M.; Sakurai, H.; Xu, Q. Au@ZIF-8: CO Oxidation over Gold Nanoparticles Deposited to Metal-Organic Framework. *J. Am. Chem. Soc.* **2009**, *131*, 11302–11303.
40. Schejn, A.; Mazet, T.; Falk, V.; Balan, L.; Aranda, L.; Medjahdib, G.; Schneider, R. Fe_3O_4@ZIF-8: Magnetically Recoverable Catalysts by Loading Fe_3O_4 Nanoparticles Inside a Zinc Imidazolate Framework. *Dalton Trans.*, **2015**, *44*, 10136-10140.
41. Yang, Q.; Xu, Q.; Yu, S.-H.; Jiang, H.-L. Pd Nanocubes@ZIF-8: Integration of Plasmon-Driven Photothermal Conversion with a Metal–Organic Framework for Efficient and Selective Catalysis. *Angew. Chem. Int. Ed.* **2016**, *55*, 3685-3689.
42. Huang, Y.; Zhang, Y.; Chen, X.; Wu, D.; Yia, Z.; Cao, R. Bimetallic Alloy Nanocrystals Encapsulated in ZIF-8 for Synergistic Catalysis of Ethylene Oxidative Degradation. *Chem. Commun.* **2014**, *50*, 10115-10117.
43. Jiang, H.-L.; Akita, T.; Ishida, T.; Haruta, M.; Xu, Q. Synergistic Catalysis of Au@Ag Core−Shell Nanoparticles Stabilized on Metal−Organic Framework. *J. Am. Chem. Soc.*, **2011**, *133*, 1304–1306
44. Li, P.-Z.; Aranishi, K.; Qiang Xu, Q. ZIF-8 Immobilized Nickel Nanoparticles: Highly Effective Catalysts for Hydrogen Generation from Hydrolysis of Ammonia Borane. *Chem. Commun.*, **2012**, *48*, 3173–3175
45. Chen, L.; Zhan, W.; Fang, H.; Cao, Z.; Yuan, C.; Xie, Z.; Kuang, Q.; Zheng, L. Selective Catalytic Performances of Noble Metal Nanoparticle@MOF Composites: The Concomitant Effect of Aperture Size and Structural Flexibility of MOF Matrices. *Chem. Eur. J.* **2017**, *23*, 11397-11403.
46. Rosler, C.; Aijaz, A.; Turner, S.; Filippousi, M.; Shahabi, A.; Xia, W.; Van Tendeloo, G.; Muhler, M.; Fischer, R. A. Hollow Zn/Co Zeolitic Imidazolate Framework (ZIF) and Yolk-Shell Metal@Zn/Co ZIF Nanostructures. *Chem. Eur. J.* **2016,** *22*, 3304-3311.
47. Yang, J.; Zhang, F.; Lu, H.; Hong, X.; Jiang, H.; Wu, Y.; Li, Y. Hollow Zn/Co ZIF Particles Derived from Core–Shell ZIF-67@ZIF-8 as Selective Catalyst for the Semi-Hydrogenation of Acetylene. *Angew. Chem. Int. Ed.* **2015,** *54*, 10889-10893.
48. Bastús, N. G.; Comenge, J.; Puntes, V. Kinetically Controlled Seeded Growth Synthesis of Citrate-Stabilized Gold Nanoparticles of up to 200 nm: Size Focusing versus Ostwald Ripening. *Langmuir* **2011**, *27*, 11098-11105.
49. Piella, J.; Bastús, N. G.; Puntes, V. Size-Controlled Synthesis of Sub-10-nanometer Citrate-Stabilized Gold Nanoparticles and Related Optical Properties. *Chem. Mater.* **2016**, *28*, 1066-1075.
50. Huang, H.; Wang, Y.; Ruditskiy, A.; Peng, H.-C.; Zhao, X.; Zhang, L.; Liu, J.; Ye, Z.; Xia, Y. Polyol Syntheses of Palladium Decahedra and Icosahedra as Pure Samples by Maneuvering the Reaction Kinetics with Additives. *ACS Nano* **2014**, *8*, 7041-7050.
51. Mézailles, N.; Ricard, L.; Gagosz, F. Phosphine Gold(I) Bis-(trifluoromethanesulfonyl)imidate Complexes as New Highly Efficient and Air-Stable Catalysts for the Cycloisomerization of Enynes. *Org. Lett.* **2005**, *7*, 4133-4136.
52. Worlikar, S. A.; Kesharwani, T.; Yao, T.; Larock, R. C. Synthesis of 3,4-Disubstituted 2*H*-Benzopyrans through C−C Bond Formation via Electrophilic Cyclization. *J. Org. Chem.* **2007**, *72*, 1347-1353.
53. Efe, C.; Lykakis, I. N.; Stratakis, M. Gold Nanoparticles Supported on TiO_2 Catalyse the Cycloisomerisation/Oxidative Dimerisation of Aryl Propargyl Ethers. *Chem. Commun.* **2011**, *47*, 803-805.
54. Lykakis, I. N.; Efe, C.; Gryparis, C.; Stratakis, M. $Ph_3PAuNTf_2$ as a Superior Catalyst for the Selective Synthesis of 2*H*-Chromenes: Application to the Concise Synthesis of Benzopyran Natural Products. *Eur. J. Org. Chem.* **2011**, 2334-2338.
55. Arcadi, A.; Blesi, F.; Cacchi, S.; Fabrizi, G.; Goggiamani, A.; Marinelli, F. Gold *versus* Silver Catalyzed Intramolecular Hydroarylation Reactions of [(3-arylprop-2-ynyl)oxy]benzene Derivatives. *Org. Biomol. Chem.* **2012**, *10*, 9700-9708.
56. Lutz, R. P. Catalysis of the Cope and Claisen rearrangements. *Chem. Rev.* **1984**, *84*, 205–247.
57. Wu, X.; Yang, C.; Ge, J. Green Synthesis of Enzyme/metal-organic framework Composites with High Stability in Protein Denaturing Solvents. *Bioresour. Bioprocess. 2017*, 4:24.

Table of Contents